Polarization of IRON-REGULATED TRANSPORTER 1 (IRT1) to the plant-soil interface plays crucial role in metal homeostasis

Marie Barberon[a], Guillaume Dubeaux[b], Cornelia Kolb[c], Erika Isono[c], Enric Zelazny[b], and Grégory Vert[b,1]

[a]Department of Plant Molecular Biology, Biophore Building, UNIL-Sorge, Université de Lausanne, 1015 Lausanne, Switzerland; [b]Institut des Sciences du Végétal, Unité Propre de Recherche 2355, Centre National de la Recherche Scientifique, 91190 Gif-sur-Yvette, France; and [c]Department of Plant Systems Biology, Technische Universität München, 85354 Freising, Germany

In plants, the controlled absorption of soil nutrients by root epidermal cells is critical for growth and development. IRON-REGULATED TRANSPORTER 1 (IRT1) is the main root transporter taking up iron from the soil and is also the main entry route in plants for potentially toxic metals such as manganese, zinc, cobalt, and cadmium. Previous work demonstrated that the IRT1 protein localizes to early endosomes/*trans*-Golgi network (EE/TGN) and is constitutively endocytosed through a monoubiquitin- and clathrin-dependent mechanism. Here, we show that the availability of secondary non-iron metal substrates of IRT1 (Zn, Mn, and Co) controls the localization of IRT1 between the outer polar domain of the plasma membrane and EE/TGN in root epidermal cells. We also identify FYVE1, a phosphatidylinositol-3-phosphate-binding protein recruited to late endosomes, as an important regulator of IRT1-dependent metal transport and metal homeostasis in plants. FYVE1 controls IRT1 recycling to the plasma membrane and impacts the polar delivery of this transporter to the outer plasma membrane domain. This work establishes a functional link between the dynamics and the lateral polarity of IRT1 and the transport of its substrates, and identifies a molecular mechanism driving polar localization of a cell surface protein in plants.

Arabidopsis | endocytosis | nutrition | radial transport | PI3P

Iron is an essential element for virtually all organisms because it plays critical roles in life-sustaining processes (1). Iron's ability to gain and lose electrons makes iron a cofactor of choice for enzymes involved in a variety of oxidation-reduction reactions, such as photosynthesis, respiration, hormone synthesis, and DNA synthesis. This essential role of iron is highlighted by the severe disorders triggered by iron deficiency, including anemia in mammals or chlorosis in plants (1). Although abundant in nature, iron is often available in limited amounts to plants because it is mostly found in rather insoluble Fe(III) complexes in soils (1). The IRON-REGULATED TRANSPORTER 1 (IRT1) root iron transporter from the model plant *Arabidopsis thaliana* takes up iron from the soil upon iron deficiency (2). IRT1 is a major player in the regulation of plant iron homeostasis, as attested by the severe chlorosis and lethality of an *irt1-1* knockout mutant (2). Consistently, *IRT1* gene is highly expressed in iron-starved root epidermal cells that face the rhizosphere (2). The resultant IRT1-dependent iron absorption allows proper growth and development under iron-limited conditions.

Despite its absolute requirement, iron reacts in cells with oxygen and generates noxious reactive oxygen species that are deleterious for plant growth and development (3). Cellular and whole-organism iron homeostasis must, therefore, be strictly balanced. Moreover, IRT1 also participates in the absorption of zinc, manganese, cobalt, and industrial pollutants such as cadmium and nickel (4–8). As such, IRT1 is the main entry route for such potentially toxic metals in iron-starved plants and in the food chain. Intricate regulatory networks control plant responses to low iron conditions and, more specifically, *IRT1*

gene expression. Several transcription factors directly binding to the *IRT1* promoter in root epidermal cells have been identified and control its inducibility by low iron conditions (9–12). Other pathways including the cytokinin-mediated root growth control and the stress hormone ethylene impinge on iron uptake by converging at the level of the *IRT1* promoter (13, 14). The integration of these regulatory networks aims at providing enough iron to sustain growth and avoid detrimental effects of iron overload.

A posttranslational control of IRT1 protein by ubiquitination was identified (15, 16). IRT1 protein was shown to localize to early endosomes/*trans*-Golgi network compartments (EE/TGN) as a result of monoubiquitin- and clathrin-dependent endocytosis and is targeted to the vacuole for degradation via late endosomes (LE) (15). The ubiquitin-mediated endocytosis of IRT1 is mediated by the IDF1 RING E3 ligase (17). IRT1 localization and ubiquitination, however, appeared to be unaffected by the availability of its primary substrate iron (15), raising the question of the biological relevance of such posttranslational control of IRT1.

In the present study, we show that the availability in secondary non-iron metal substrates of IRT1 (i.e., Zn, Mn, and Co) controls its localization between the outer polar domain of the plasma membrane and EE/TGN in root epidermal cells. We identified a previously uncharacterized phosphatidylinositol-3-phosphate (PI3P)-binding protein recruited to LE, FYVE1, as an important regulator of IRT1-dependent metal transport and metal homeostasis. FYVE1 controls IRT1 recycling to the plasma membrane and impacts the polar delivery of this transporter to the outer plasma membrane domain. This work establishes a functional

Significance

Plants take up iron from the soil by using a broad spectrum transporter named IRON-REGULATED TRANSPORTER 1 (IRT1). IRT1 mediates influx of potentially toxic elements such as manganese, zinc, cobalt, and cadmium. We uncovered that the localization at the cell surface of IRT1 is directly controlled by its secondary toxic substrates. When these metals are found at low levels in soils, IRT1 is located at the plasma membrane in a polar fashion facing the soil. We identified a lipid-binding protein recruited to endosomes that controls IRT1's dynamics and polarity, and plays an important role in the radial transport of metals. Altogether, our work points to an unexpected mode of radial transport of iron toward vascular tissues involving efflux transporters.

PLANT BIOLOGY

link between the dynamics and the lateral polarity of IRT1 and the transport of its substrates, and identifies a molecular mechanism driving outer polar localization of a cell surface protein in plants.

Results and Discussion

The root iron transporter IRT1 undergoes Ub-dependent endocytosis, although this process is not regulated by the availability in iron, its primary substrate (15). To get further insight into the mechanisms driving IRT1 localization in EE/TGN, we tested the influence of the secondary metal substrates of IRT1 by immunolocalization using anti-IRT1–specific antibodies on plants constitutively expressing *IRT1*. Although IRT1 localized under standard conditions to intracellular vesicles that we previously characterized as EE/TGN (15), depletion of non-iron metal substrates of IRT1 led to its accumulation at the cell surface of root hairs (Fig. 1*A*). The EE/TGN identity was not altered by non-iron metal deficiency because known EE/TGN markers failed to relocalize to the cell surface under such growth conditions in differentiated root cells where *IRT1* is expressed (Fig. S1*A*) (18, 19). These observations highlight the ability of potentially toxic non-iron metals transported by IRT1 to specifically trigger its intracellular dynamics between the cell surface and EE/TGN. The nonubiquitinatable $IRT1_{K154RK179R}$ was found at the cell surface in the presence of metals, as reported (15), providing genetic evidence that the response to the secondary substrates of IRT1 is likely mediated by Ub-mediated endocytosis (Fig. 1*A*). Metal-dependent endocytosis appears as a protective mechanism to limit the absorption of the secondary substrates of IRT1. Indeed, depletion of Mn, for example, from the medium alleviates the deleterious consequences of $IRT1_{K154RK179R}$ expression (Fig. 1*B*). Under iron limitation where *IRT1* is strongly expressed, non-iron metals are readily available for transport by IRT1 and are heavily accumulated (2). In contrast, iron is not efficiently taken up because of its low level and the necessity of reduction by the FRO2 reductase whose activity is limiting for iron transport (20). Taken together, these observations point to the existence of multiple layers of regulation by metals for *IRT1* gene expression. Iron indeed controls *IRT1* transcription, whereas its secondary non-iron metal substrates act at the posttranscriptional level, as observed for Zn (21), and at the posttranslational level on the dynamics of IRT1 protein.

We also monitored IRT1 localization in response to metals in root epidermal cells. Interestingly, IRT1 accumulated under metal-depleted conditions at the outer polar domain of the plasma membrane facing the rhizosphere (Fig. 1*C*). Quantification of IRT1 fluorescence, represented as the fluorescence profile across root epidermal cells (Fig. S1*B*) or as the ratio between outer and inner plasma membrane fluorescence intensities (Fig. 1*D*), show a clear enrichment of IRT1 in the outer plasma membrane domain. Lateral polarity in plant roots was described first in rice for the As/Si transporters Lsi1, Lsi2 (22), and in *Arabidopsis* for the boron transporter BOR4 (23). Then an increasing number of transporters were demonstrated to be laterally polarized in *Arabidopsis* roots such PDR8/PEN3, BOR1, NIP5;1, PIS1/PDR9/ABCG37, and NRT2.4 (24–28). However, the molecular mechanisms controlling lateral polarity are still unclear. To shed light on the mechanisms controlling IRT1 metal-dependent dynamics and its localization at the outer plasma membrane domain of root epidermal cells, we investigated the localization of the nonubiquitinatable $IRT1_{K154RK179R}$ mutant version. $IRT1_{K154RK179R}$ localized to the outer polar domain in the presence of metals, similar to what is observed with wild-type IRT1 under non-iron metal depleted conditions (Fig. 1 *C* and *D* and Fig. S1*B*). We demonstrated that IRT1 accumulates at the cell surface in root hair cells when clathrin-mediated endocytosis (CME) is impaired (15). Inhibition of CME in root epidermal cells, due to tamoxifen-inducible expression of a dominant-negative clathrin form, led to the redistribution of IRT1 at the outer plasma membrane domain (Fig. 1 *C* and *D* and Fig. S1*B*). The same DN-HUB1 line prevented the
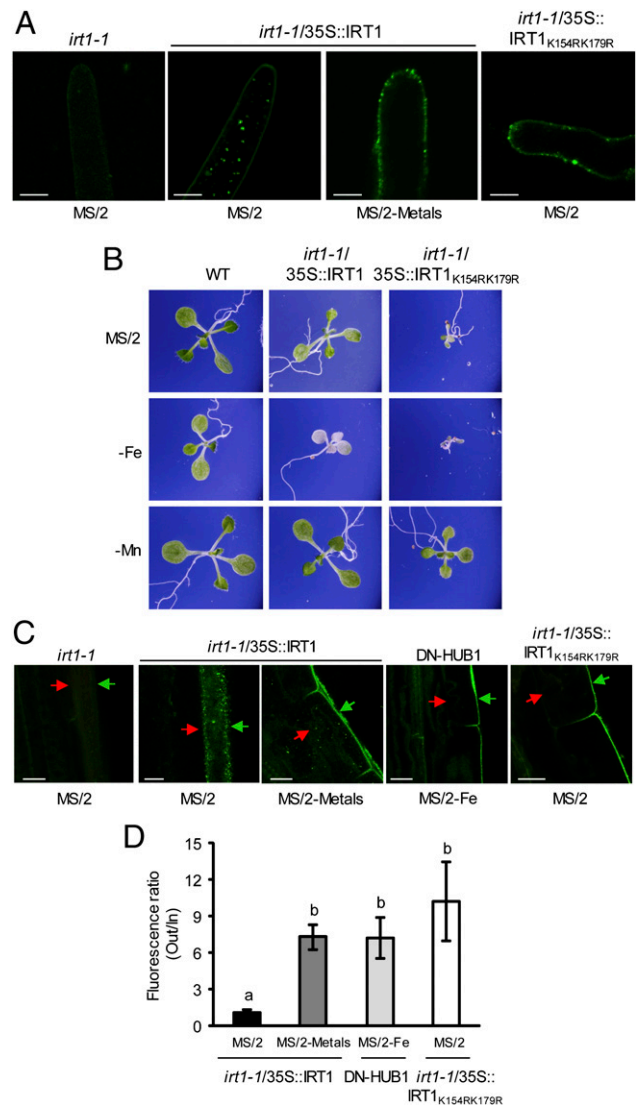

Fig. 1. IRT1 localization to the outer polar domain in low metal conditions. (*A*) IRT1 immunolocalization with anti-IRT1 antibodies on root hair cells of *irt1-1*, *irt1-1/35S*::IRT1, and *irt1-1/35S*::IRT1$_{K154RK179R}$ plants grown 7 d in different metal conditions. MS/2 refers to standard plant growth medium containing metals. Metal depleted conditions correspond to combined absence of Zn, Mn, and Co. (*B*) Phenotype of wild-type, *irt1-1/35S*::IRT1, and *irt1-1/35S*::IRT1$_{K154RK179R}$ plants grown on standard medium (MS/2), iron- (-Fe), and manganese-depleted media (-Mn). (*C*) IRT1 immunolocalization with anti-IRT1 antibodies on root epidermal cells of *irt1-1*, *irt1-1/35S*::IRT1, tamoxifen-induced DN-HUB1, and *irt1-1/35S*::IRT1$_{K154RK179R}$ plants grown 7 d in different metal conditions. DN-HUB1 plants express an inducible dominant-negative clathrin HUB and are defective in CME. Red and green arrows mark the inner and outer plasma membrane domains of root epidermal cells (PM$_{in}$ and PM$_{out}$) used for quantification of polarity profiles (Fig. S1*B*). (*D*) Quantification of the outer/inner polarity ratios in root epidermal cells. Data represents the mean ± SE (*n* = 10). Different letters indicate means that were statistically different by one-way ANOVA and Tukey's multiple testing method (*P* < 0.05). Ratio = 1 indicates apolar plasma membrane localization, or nonplasma membrane localization in the case of wild-type plants, ratio < 1 indicates inner localization, and ratio >1 indicates outer localization. (Scale bars: 10 μm.)

accumulation of the BRI1 steroid hormone receptor in endosomal aggregates triggered by the fungal toxin brefeldin A (BFA) upon induction, ensuring that DN-HUB1 effectively inhibited CME (Fig. S1*C*). These results indicate that the presence of IRT1 in the outer plasma membrane polar domain is established independently of IRT1 ubiquitination and CME.

To identify factors involved in the control of IRT1 localization, we performed a yeast two-hybrid screen by using the hydrophilic cytosolic loop of IRT1 as bait. This screen identified several clones of an uncharacterized FYVE domain-containing protein named FYVE1 (Fig. 2A) (29). Expression analyses confirmed that *FYVE1* transcripts are found in roots, similar to *IRT1*, although not regulated by iron starvation (Fig. S2A). To further confirm the protein–protein interaction between FYVE1 and IRT1, we first generated transgenic plants expressing FYVE1-mCitrine in the wild-type background. Using anti-GFP antibodies, FYVE1-mCitrine was immunoprecipitated from wild-type or FYVE1-mCitrine iron-deficient plants where *IRT1* is expressed. The presence of IRT1 was only observed in immunoprecipitates from FYVE1-mCitrine (Fig. 2B), attesting that both proteins are able to interact in vivo.

FYVE domains have been reported to recognize PI3P, leading to recruitment of FYVE domain-containing proteins to EE and LE (30–34). To assess whether FYVE1 binds to PI3P, we performed lipid overlay analyses by using in vitro-transcribed/translated FYVE1-FLAG. FYVE1 interacted with PI3P, in agreement with previous reports on FYVE domain-containing proteins, and other acidic phospholipids, although to a lesser extent (Fig. 2C). Confocal microscopy imaging of FYVE1-mCitrine showed that FYVE1 protein is found in the nucleus, the cytosol, and in intracellular vesicles that may correspond to LE in root tip cells (Fig. S2B) and in differentiated root cells (Fig. 2D), although more difficult to visualize because of the large central vacuole. We further investigated FYVE1 localization in differentiated epidermal cells where *IRT1* is expressed, and in root tip cells because they allow easy visualization of intracellular compartments, are readily accessible to drug and dye treatments, and have been extensively characterized (35). The recruitment of FYVE1 to LE was confirmed by its sensitivity to the inhibitor of PI3-kinase Wortmannin, which creates homotypic fusion and swelling of LE (Fig. 2E and Fig. S2C) (36). Consistently, FYVE1-mCitrine showed colocalization with the LE marker RabF2a (Fig. 2 F and H and Fig. S2 D and F) and the PI3P-recruited and LE-localized 2xFYVE_{HRS} (Fig. 2 G and H and Fig. S2 E and F). Altogether those results demonstrate that IRT1 interacts with the LE-recruited and PI3P-binding protein FYVE1.

To functionally characterize FYVE1, we isolated the publicly available pst18264 RIKEN insertion line, hereafter named *fyve1-1*. This line carries the *DS* transposon in the first exon of the *FYVE1* gene. We repeatedly failed to identify homozygous *fyve1-1* knockout mutants in the progeny of *fyve1-1* heterozygous plants, suggesting that the corresponding mutation is likely lethal at the homozygous state. Consistently, *fyve1-1* segregating mutants produced approximately 26% of seeds that failed to germinate, corresponding to the ratio expected for plants segregating a recessive mutation impairing germination (Table 1). Genetic complementation of *fyve1-1* was carried out by crossing heterozygous *fyve1-1* mutant with a monoinsertional segregating line constitutively expressing Ubi10::FYVE1. The progeny now only showed 6.9% of seeds that failed to germinate, matching the expected segregation of 6.25% for plants carrying the homozygous *fyve1-1* mutation and that do not possess transgenic *FYVE1* (Table 1). Homozygous *fyve1-1* mutants carrying Ubi10::FYVE1 were also recovered in the progeny (Fig. S3A), further highlighting the genetic complementation of *fyve1-1* by *FYVE1*. Overall, this genetic analysis clearly demonstrates that the loss-of-function mutation in the *FYVE1* gene is the direct cause of *fyve1-1* lethality. Because the onset of *IRT1* expression is at 3 d after germination, we cannot use *fyve1-1* to address the biological role of FYVE1 in iron homeostasis. We therefore generated transgenic plants constitutively expressing *FYVE1* under the control of the strong 35S promoter, leading to overaccumulation of *FYVE1* transcripts in transgenic plants (Fig. S3B). Such plants showed no phenotype when grown in the presence of iron in the medium (Fig. 3 A and B). When grown on iron-depleted media, 35S::FYVE1 plants displayed shorter roots than wild type (Fig. 3 A and B),
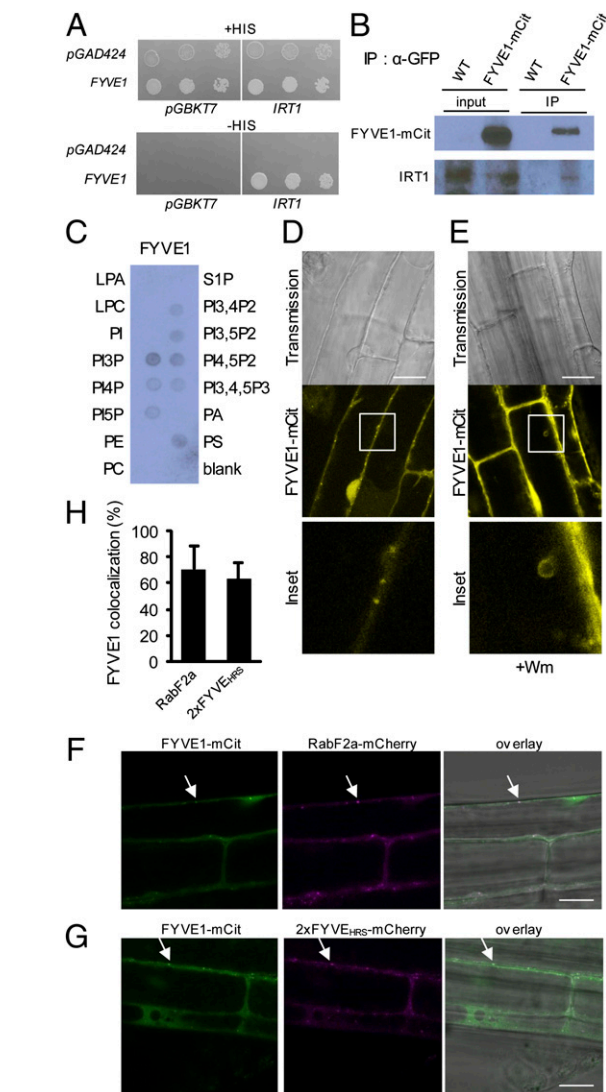

Fig. 2. FYVE1 interacts with IRT1 and PI3P and is recruited to late endosomes. (A) Yeast two-hybrid screening using IRT1 as bait identified FYVE1. The interaction is revealed by the activation of *HIS3* transcription and growth on -HIS medium. (B) Coimmunoprecipitation analyses between FYVE1-mCitrine and IRT1 in iron-deficient roots. (C) Lipid binding assays of in vitro transcribed/translated FYVE1 protein. LPA, lysophosphatidic acic; LPC, lysophosphatidylcholine; PA, phosphatidic acid; PC, phosphatidylcholine; PE, phosphatidylethanolamine; PI, phosphatidylinositol; PI3P, PI-3-phosphate; PI3,4P2, PI-3,4-bisphosphate; PI3,4,5P3, PI-3,4,5-triphosphate; PI3,5P2, PI-3,5-bisphosphate; PI4P, PI-4-phosphate; PI4,5P2, PI-4,5-bisphosphate; PI5P, PI-5-phosphate; PS, phosphatidylserine; S1P, sphingosine-1-phosphate. (D) Localization of FYVE1-mCitrine fusion protein in differentiated root cells. (E) Sensitivity of FYVE1-mCitrine trafficking to Wortmannin (Wm) in differentiated root cells. (F and G) Colocalization of FYVE-mCitrine with the late endosomal marker RabF2a-mCherry (F) and 2xFYVE_{HRS}-mCherry (G) in differentiated root cells. Arrows show an example of colocalization. Scale bar, 10μm. (H) Quantification of FYVE1 colocalization with the late endosomal markers RabF2a and 2xFYVE_{HRS}. Colocalization of punctate structures was quantified in 10 cells from the F_1 progeny from crosses between parental lines FYVE1-mCitrine and marker lines RabF2a and 2xFYVE_{HRS}. Data represents the mean ± SE. (Scale bars: 10 μm.)

a hallmark of iron-deficient plants. The hypersensitivity of 35S::FYVE1 plants to low iron conditions is abolished when plants are grown on medium containing Wortmannin (Fig. S3C), indicating that PI3P is necessary for the role of FYVE1 in iron homeostasis. Plants overexpressing the well-established PI3P-binding 2xFYVE_{HRS} reporter showed wild-type sensitivity

Table 1. *fyve1-1* germination phenotype and genetic complementation

Parental genotype	Germinated, %	Ungerminated, %	n	χ^2	P value
WT	97.7	2.3	176		
fyve1/FYVE1	70.9	29.1	617	2.628	0.019*
fyve1/FYVE1 Ubi10::FYVE1 [+/−]	91.8	9.2	455	2.634	0.011*
fyve1/FYVE1 (corrected)	73.2	26.8	617	0.390	0.373
fyve1/FYVE1 Ubi10::FYVE1 [+/−] (corrected)	93.1	6.9	455	0.037	0.729

Segregation of the progeny phenotypes (germinated:ungerminated) were corrected for the germination defect of wild-type (WT) Nossen ecotype and evaluated with the χ^2 goodness-of-fit test by using 3:1 segregation as a null hypothesis for *fyve1* and 15:1 segregation as a null hypothesis for *fyve1* Ubi10::FYVE1. χ^2 values (χ^2) and corresponding P values are indicated. *Significant difference ($P < 0.05$).

to low iron, attesting the specific involvement of FYVE1 in plant responses to low iron (Fig. 3 *A* and *B*) (34). To further evaluate the biological role of FYVE1 in metal homeostasis, we determined the metal content of both wild-type and 35S::FYVE1 plants by Inductively-Coupled Plasma Mass Spectrometry (ICP-MS). Under metal-replete conditions, both wild-type and 35S::FYVE1 plants showed comparable metal accumulation profile (Fig. 3*C*). When grown in the absence of iron, however, 35S::FYVE1 roots accumulated slightly less Fe and showed signifi-

Fig. 3. *FYVE1* overexpression leads to iron deficiency and impaired transport of IRT1 substrates. (*A*) Phenotype of wild-type (WT), two independent 35S:FYVE1, and two independent 35S::2xFYVE_HRS transgenic lines grown 5 d in +Fe (*Upper*) or in -Fe (*Lower*). (*B*) Root length of 5-d-old wild-type (WT), 35S:FYVE1, and 35S::2xFYVE_HRS grown with or without Fe. Results are presented as mean ± SD ($n = 20$). Statistical differences were calculated by one-way ANOVA. Different letters indicate means that were statistically different by Tukey's multiple testing method ($P < 0.05$). (*C*) Metal content determined by ICP-MS on roots of 7-d-old plants grown with or without Fe. Results are presented as mean ± SD from three to four batches of 30 seedlings. Statistical differences were calculated by one-way ANOVA. Different letters indicate means that were statistically different by Tukey's multiple testing method ($P < 0.05$) for genotypes within a given growth condition (+Fe or -Fe).

cantly reduced levels of non-iron IRT1 substrates. As a control, we monitored accumulation of boron that is not transported by IRT1 and observed no difference between the two genotypes (Fig. 3*C*).

The fact that 35S::FYVE1 showed hypersensitivity to low iron growth conditions and reduced accumulation of metals transported by IRT1 prompted us to investigate IRT1 expression in both wild-type and 35S::FYVE1 plants. *FYVE1*-overexpressing plants accumulated wild-type levels of IRT1 protein (Fig. 4*A*), indicating that the phenotypes displayed by 35S::FYVE1 plants are not explained by lower accumulation of IRT1 transporter. We then analyzed IRT1 protein localization by immunolocalization to highlight possible defects in IRT1 localization. Wild-type plants grown in the absence of iron showed strong accumulation of IRT1 in EE/TGN, as reported (15), whereas *FYVE1* over-expressors readily accumulated IRT1 at the plasma membrane in a nonpolar fashion (Fig. 4*B*). The ratio of plasma membrane fluorescence intensity out/in is 1 for both genotypes (Fig. 4*C*), although corresponding to intracellular EE/TGN and apolar plasma membrane localization, respectively. However, quantification of fluorescence profiles across root epidermal cells clearly argues for IRT1 accumulating at the plasma membrane in a nonpolar fashion in 35S::FYVE1 plants (Fig. 4*B*). *FYVE1* overexpression therefore affects IRT1 localization between the plasma membrane and EE/TGN, and its polarity on the plasma membrane. The presence of IRT1 at the cell surface in 35S::FYVE1 transgenic plants is not explained by a defect in general endocytosis because both wild-type and 35S::FYVE1 show comparable internalization of the endocytic tracer FM4-64 in both root tip and differentiated cells (Fig. S3 *D and E*). Taken together, these observations suggest that FYVE1 acts more on the recycling of IRT1 from endosomal compartments back to the plasma membrane.

The polar localization of PIN proteins at the apico-basal domain of root cells requires clearance from the PM by endocytosis involving clathrin (37, 38), retargeting to and retention at the polar domain (39, 40). Similarly, possible tyrosine-based motifs have been involved in the lateral polarity of BOR1, suggesting a role for endocytosis that depends on clathrin in this process (27). CME appears not to be required for IRT1 polarization, as evidenced by the lateral polarity of IRT1 in DN-HUB1 transgenic plants (Fig. 1 *C* and *D* and Fig. S1*B*). Our work rather points to the role for the LE-recruited PI3P-binding FYVE1 protein in the recycling of IRT1 from endosomal compartments. Although the ability of LE to function in recycling has been debated in the recent years (41, 42), the presence of vacuolar sorting receptors (43) and retromer subunits (44) in LE suggest a function as a recycling compartment (45–47). Over-expression of *FYVE1* may therefore misroute IRT1 beyond the outer polar plasma membrane domain on its way back to the cell surface.

We reported that IRT1 mislocalization at the plasma membrane, resulting from impaired ubiquitination of IRT1, leads to severe growth defects and oxidative stress due to metal toxicity (15). In this particular case, IRT1$_{K154RK179R}$ showed lateral polarity, as observed for endogenous IRT1 protein (Fig. 1 *C* and
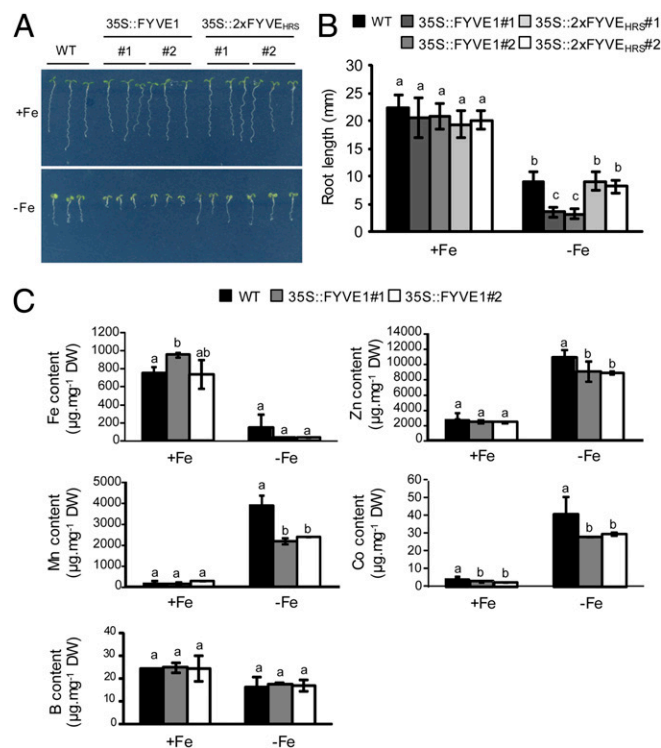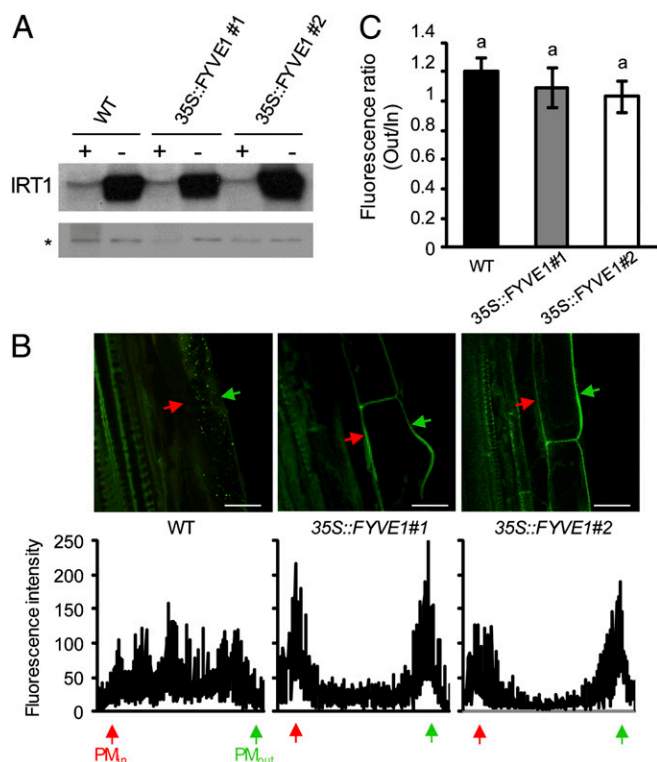
Fig. 4. *FYVE1* overexpression leads to apolar IRT1 accumulation at the cell surface. (*A*) IRT1 protein accumulation in roots of 7-d-old wild-type (WT) and 35S::FYVE1 independent transgenic lines grown in the presence (+) or absence (−) of Fe. Total protein were extracted and analyzed by Western blot with anti-IRT1 antibodies. The nonspecific band indicated with an asterisk serves as a loading control. (*B*) IRT1 immunolocalization with anti-IRT1 antibodies, in differentiated roots of wild-type (WT) and 35S::FYVE1 plants grown in Fe-deficient conditions. (Scale bars: 10 μm.) Red and green arrows mark the inner and outer plasma membrane domains of root epidermal cells (PM_{in} and PM_{out}), respectively. Quantification of polarity profiles across corresponding epidermal cells is shown below each image and represents the best fitted curve from independent immunofluorescence experiments ($n = 10$). (*C*) Quantification of the outer/inner polarity ratios in differentiated root epidermal cells. Data represents the mean ± SE ($n = 10$). Statistical differences were calculated by one-way ANOVA. Different letters indicate means that were statistically different by Tukey's multiple testing method ($P < 0.05$). Ratio = 1 indicates apolar localization or nonplasma membrane localization in the case of wild-type plants, ratio < 1 indicates inner localization, and ratio >1 indicates outer localization.

D and Fig. S1*B*). We now observe that the apolar presence of IRT1 at the cell surface leads to metal deficiency (Figs. 3 and 4 *B* and *C*). A possible explanation is that, although accumulating at the plasma membrane in 35S::FYVE1, IRT1 has decreased transport activity. Impaired metal transport may, for example, result from IRT1 being localized to different membrane subdomains in 35S::FYVE1, or lacking a partner or posttranslational modification required for full transport activity. Alternatively, a tantalizing hypothesis is that the polarity of IRT1 is critical for proper radial transport of metal in the root. We demonstrated that the vast majority of iron is taken up by root epidermal cells (2). Whether iron is transported from epidermal cells to underlying cortical cells symplasmically using cell-cell connections called plasmodesmata or via efflux transporters remains elusive. Our observations showing that IRT1 polarity is critical for iron and metal homeostasis suggest that these metals exit root epidermal cells using efflux transporters rather than the symplasmic route. The loss of polarity would result in IRT1 working against such efflux transporter, leading to radial transport defects within the root and, thus, impaired metal accumulation.

This hypothesis is supported by several studies based on dye-coupling approaches showing that differentiated root epidermal and root hair cells of several plant species including *A. thaliana* are symplasmically isolated from neighboring cells (48, 49). Although one can argue that dyes used in these studies may have a larger radius than many hydrated ions, most highly reactive metals appear to be chelated to various organic molecules (i.e., nicotianamine, citrate) and metallochaperones in the cell (1, 50). Altogether, the lack of symplasmic transport between epidermal and underlying cortical cells, associated to the specific requirement for a polar localization of IRT1, strongly suggest that iron and metals transported by IRT1 exits epidermal cells by using efflux transporters. Homologs of mammalian metal efflux transporters from the IREG/ferroportin family have been described in *Arabidopsis* and play a role in metal homeostasis (51, 52). Whether such proteins play a role in iron and metal exit from epidermal cells will have to be addressed in the future.

In plants, the necessity of a functional interface between the root and the soil is obvious, but virtually nothing is defined. Here, we demonstrated that the localization of the IRT1 root iron transporter is dynamically controlled between the EE/TGN and the cell surface by its potentially toxic secondary substrates to avoid non-iron metal toxicity. In addition, we identified an endosomal-recruited protein controlling not only the localization but also the polarity of IRT1, and, thus, establishing the functional link between lateral polarity of a transporter and transport of its substrate. Finally, our work also opens the door to a better understanding on the establishment of polarity for other proteins targeted to the outer plasma membrane domain and acting as nutrient and hormone transporters or mediators of pathogen defense (22–25, 27, 28).

Methods

Materials and Growth Cconditions. Wild-type and the various transgenic lines used in this study were grown in sterile conditions on vertical plates at 21 °C with 16-h light/8-h dark cycles, as described (14). For expression analyses, plants were cultivated in the conditions described above for 7 d and then transferred on iron-sufficient (50 μM Fe-EDTA) or iron-deficient (300 μM Ferrozine [3-(2-pyridyl)-5,6-diphenyl-1,2,4-triazine sulfonate], a strong iron chelator) medium for an additional 3 d. For immunolocalization studies, iron starvation was applied by directly germinating seeds on half-strength Murashige and Skoog (MS) medium lacking exogenous iron to preserve root integrity. All reagents were purchased from Sigma-Aldrich.

The *irt1-1*, *irt1-1/35S::IRT1*, *irt1-1/35S::IRT1*$_{K154RK179R}$, dominant negative clathrin hub DN-HUB1, RabF2a-mCherry, 2xFYVE$_{HRS}$-mCherry, 2xFYVE$_{HRS}$, BRI1-mCitrine, VHAa1-GFP, and VTI112-YFP lines were described in previous studies (2, 15, 18, 19, 34, 37, 53, 54). The *fyve1-1* insertion mutant (pst18264, Nossen ecotype) was isolated from the RIKEN collection. Genotyping of *fyve1-1* was carried out with the primers listed in *SI Methods*.

The *FYVE1* ORF was cloned into pCHF3 binary vector under the control of 35S promoter, or recombined by multisite Gateway technology to generate Ubi10::FYVE1-mCitrine in the pB7m34GW binary vector. For lipid binding assays, FYVE1 was recombined in pTnT GW-HF, a gateway compatible in vitro transcription/translation vector carrying a FLAG tag (55).

Imaging. FM4-64 (Invitrogen) was applied at a concentration of 5 μM; Cycloheximide (Sigma-Aldrich) was applied at a concentration of 100 μM for 1 h before treatment with BFA; BFA and Wortmannin (Sigma-Aldrich) were applied at a concentration of 50 μM and 33 μM for 1 h in liquid medium, respectively.

Imaging was performed on an inverted Leica SP2 and Zeiss 700 confocal microscopes. The percentage of FYVE1-mCitrine dotted structures showing overlap with RabF2a-mCherry or 2xFYVE$_{HRS}$-mCherry was manually determined. Induction of DN-HUB1 was performed with 2 μM 2-hydroxytamoxifen for 24 h. For polarity profiles, epidermal cell width was normalized and fluorescence intensity determined across cells with ImageJ. Intensity values as a function of distance were plotted for each experiment, and the moving average was applied to the scatterplot. The ratios between outer (PM_{out}) and inner (PM_{in}) plasma membrane domains were determined with ImageJ. For FM4-64 internalization assays, z stacks encompassing the whole cell volume were acquired every 5 min until internalization is observed. Three independent experiments obtained 25 min after FM4-64

addition were analyzed by using ImageJ. To better visualize the endosomes, images were treated with the Difference of Gaussian filter, and the number of FM4-64–positive endosomes in a cell was quantified on the treated images by using the 3D Object Counter plugin of ImageJ.

Elemental Analyses. Tissues were desorbed by washing for 10 min with 2 mM $CaSO_4$ and 10 mM EDTA and then rinsed for 5 min with deionized water. Samples were dried at 80 °C for 2 d. For mineralization, tissues were digested completely (1–3 h) in 70% (vol/vol) HNO_3 at 120 °C. Elemental analyses were performed by ICP-MS.

1. Kobayashi T, Nishizawa NK (2012) Iron uptake, translocation, and regulation in higher plants. *Annu Rev Plant Biol* 63:131–152.
2. Vert G, et al. (2002) IRT1, an Arabidopsis transporter essential for iron uptake from the soil and for plant growth. *Plant Cell* 14(6):1223–1233.
3. Thomine S, Vert G (2013) Iron transport in plants: Better be safe than sorry! *Curr Opin Plant Biol* 16(3):322–327.
4. Eide D, Broderius M, Fett J, Guerinot ML (1996) A novel iron-regulated metal transporter from plants identified by functional expression in yeast. *Proc Natl Acad Sci USA* 93(11):5624–5628.
5. Korshunova YO, Eide D, Clark WG, Guerinot ML, Pakrasi HB (1999) The IRT1 protein from Arabidopsis thaliana is a metal transporter with a broad substrate range. *Plant Mol Biol* 40(1):37–44.
6. Nishida S, et al. (2011) AtIRT1, the primary iron uptake transporter in the root, mediates excess nickel accumulation in Arabidopsis thaliana. *Plant Cell Physiol* 52(8):1433–1442.
7. Rogers EE, Eide DJ, Guerinot ML (2000) Altered selectivity in an Arabidopsis metal transporter. *Proc Natl Acad Sci USA* 97(22):12356–12360.
8. Vert G, Briat JF, Curie C (2001) Arabidopsis IRT2 gene encodes a root-periphery iron transporter. *Plant J* 26(2):181–189.
9. Colangelo EP, Guerinot ML (2004) The essential basic helix-loop-helix protein FIT1 is required for the iron deficiency response. *Plant Cell* 16(12):3400–3412.
10. Jakoby M, Wang HY, Reidt W, Weisshaar B, Bauer P (2004) FRU (BHLH029) is required for induction of iron mobilization genes in Arabidopsis thaliana. *FEBS Lett* 577(3):528–534.
11. Wang N, et al. (2013) Requirement and functional redundancy of Ib subgroup bHLH proteins for iron deficiency responses and uptake in Arabidopsis thaliana. *Mol Plant* 6(2):503–513.
12. Yuan YX, Zhang J, Wang DW, Ling HQ (2005) AtbHLH29 of Arabidopsis thaliana is a functional ortholog of tomato FER involved in controlling iron acquisition in strategy I plants. *Cell Res* 15(8):613–621.
13. Lingam S, et al. (2011) Interaction between the bHLH transcription factor FIT and ETHYLENE INSENSITIVE3/ETHYLENE INSENSITIVE3-LIKE1 reveals molecular linkage between the regulation of iron acquisition and ethylene signaling in Arabidopsis. *Plant Cell* 23(5):1815–1829.
14. Séguéla M, Briat JF, Vert G, Curie C (2008) Cytokinins negatively regulate the root iron uptake machinery in Arabidopsis through a growth-dependent pathway. *Plant J* 55(2):289–300.
15. Barberon M, et al. (2011) Monoubiquitin-dependent endocytosis of the iron-regulated transporter 1 (IRT1) transporter controls iron uptake in plants. *Proc Natl Acad Sci USA* 108(32):E450–E458.
16. Kerkeb L, et al. (2008) Iron-induced turnover of the Arabidopsis IRON-REGULATED TRANSPORTER1 metal transporter requires lysine residues. *Plant Physiol* 146(4):1964–1973.
17. Shin LJ, et al. (2013) IRT1 degradation factor1, a ring E3 ubiquitin ligase, regulates the degradation of iron-regulated transporter1 in Arabidopsis. *Plant Cell* 25(8):3039–3051.
18. Dettmer J, Hong-Hermesdorf A, Stierhof YD, Schumacher K (2006) Vacuolar H+-ATPase activity is required for endocytic and secretory trafficking in Arabidopsis. *Plant Cell* 18(3):715–730.
19. Geldner N, et al. (2009) Rapid, combinatorial analysis of membrane compartments in intact plants with a multicolor marker set. *Plant J* 59(1):169–178.
20. Connolly EL, Campbell NH, Grotz N, Prichard CL, Guerinot ML (2003) Overexpression of the FRO2 ferric chelate reductase confers tolerance to growth on low iron and uncovers posttranscriptional control. *Plant Physiol* 133(3):1102–1110.
21. Connolly EL, Fett JP, Guerinot ML (2002) Expression of the IRT1 metal transporter is controlled by metals at the levels of transcript and protein accumulation. *Plant Cell* 14(6):1347–1357.
22. Ma JF, et al. (2007) An efflux transporter of silicon in rice. *Nature* 448(7150):209–212.
23. Miwa K, et al. (2007) Plants tolerant of high boron levels. *Science* 318(5855):1417–1417.
24. Langowski L, Růžicka K, Naramoto S, Kleine-Vehn J, Friml J (2010) Trafficking to the outer polar domain defines the root-soil interface. *Curr Biol* 20(10):904–908.
25. Strader LC, Bartel B (2009) The Arabidopsis PLEIOTROPIC DRUG RESISTANCE8/ABCG36 ATP binding cassette transporter modulates sensitivity to the auxin precursor indole-3-butyric acid. *Plant Cell* 21(7):1992–2007.
26. Alassimone J, Naseer S, Geldner N (2010) A developmental framework for endodermal differentiation and polarity. *Proc Natl Acad Sci USA* 107(11):5214–5219.
27. Takano J, et al. (2010) Polar localization and degradation of Arabidopsis boron transporters through distinct trafficking pathways. *Proc Natl Acad Sci USA* 107(11):5220–5225.
28. Kiba T, et al. (2012) The Arabidopsis nitrate transporter NRT2.4 plays a double role in roots and shoots of nitrogen-starved plants. *Plant Cell* 24(1):245–258.
29. van Leeuwen W, Okrész L, Bögre L, Munnik T (2004) Learning the lipid language of plant signalling. *Trends Plant Sci* 9(8):378–384.
30. Burd CG, Emr SD (1998) Phosphatidylinositol(3)-phosphate signaling mediated by specific binding to RING FYVE domains. *Mol Cell* 2(1):157–162.
31. Gaullier JM, Ronning E, Gillooly DJ, Stenmark H (2000) Interaction of the EEA1 FYVE finger with phosphatidylinositol 3-phosphate and early endosomes. Role of conserved residues. *J Biol Chem* 275(32):24595–24600.
32. Gaullier JM, et al. (1998) FYVE fingers bind PtdIns(3)P. *Nature* 394(6692):432–433.
33. Gillooly DJ, et al. (2000) Localization of phosphatidylinositol 3-phosphate in yeast and mammalian cells. *EMBO J* 19(17):4577–4588.
34. Vermeer JEM, et al. (2006) Visualization of PtdIns3P dynamics in living plant cells. *Plant J* 47(5):687–700.
35. Jaillais Y, Gaude T (2007) Sorting out the sorting functions of endosomes in Arabidopsis. *Plant Signal Behav* 2(6):556–558.
36. Jaillais Y, Fobis-Loisy I, Miège C, Rollin C, Gaude T (2006) AtSNX1 defines an endosome for auxin-carrier trafficking in Arabidopsis. *Nature* 443(7107):106–109.
37. Dhonukshe P, et al. (2007) Clathrin-mediated constitutive endocytosis of PIN auxin efflux carriers in Arabidopsis. *Curr Biol* 17(6):520–527.
38. Kitakura S, et al. (2011) Clathrin mediates endocytosis and polar distribution of PIN auxin transporters in Arabidopsis. *Plant Cell* 23(5):1920–1931.
39. Kleine-Vehn J, Friml J (2008) Polar targeting and endocytic recycling in auxin-dependent plant development. *Annu Rev Cell Dev Biol* 24:447–473.
40. Kleine-Vehn J, et al. (2011) Recycling, clustering, and endocytosis jointly maintain PIN auxin carrier polarity at the plasma membrane. *Mol Syst Biol* 7:540.
41. Niemes S, et al. (2010) Sorting of plant vacuolar proteins is initiated in the ER. *Plant J* 62(4):601–614.
42. Viotti C, et al. (2010) Endocytic and secretory traffic in Arabidopsis merge in the trans-Golgi network/early endosome, an independent and highly dynamic organelle. *Plant Cell* 22(4):1344–1357.
43. Tse YC, et al. (2004) Identification of multivesicular bodies as prevacuolar compartments in Nicotiana tabacum BY-2 cells. *Plant Cell* 16(3):672–693.
44. Oliviusson P, et al. (2006) Plant retromer, localized to the prevacuolar compartment and microvesicles in Arabidopsis, may interact with vacuolar sorting receptors. *Plant Cell* 18(5):1239–1252.
45. Foresti O, Denecke J (2008) Intermediate organelles of the plant secretory pathway: Identity and function. *Traffic* 9(10):1599–1612.
46. Jaillais Y, Fobis-Loisy I, Miège C, Gaude T (2008) Evidence for a sorting endosome in Arabidopsis root cells. *Plant J* 53(2):237–247.
47. Otegui MS, Spitzer C (2008) Endosomal functions in plants. *Traffic* 9(10):1589–1598.
48. Duckett C, Oparka K, Prior D, Dolam L, Roberts K (1994) Dye-coupling in the root epidermis of Arabidopsis is progressively reduced during development. *Development* 120:3247–3255.
49. Erwee MG, Goodwin PB (1985) Symplast domains in extrastelar tissues of Egeria densa Planch. *Planta* 163(1):9–19.
50. Puig S, Peñarrubia L (2009) Placing metal micronutrients in context: Transport and distribution in plants. *Curr Opin Plant Biol* 12(3):299–306.
51. Morrissey J, et al. (2009) The ferroportin metal efflux proteins function in iron and cobalt homeostasis in Arabidopsis. *Plant Cell* 21(10):3326–3338.
52. Schaaf G, et al. (2006) AtIREG2 encodes a tonoplast transport protein involved in iron-dependent nickel detoxification in Arabidopsis thaliana roots. *J Biol Chem* 281(35):25532–25540.
53. Jaillais Y, et al. (2011) Tyrosine phosphorylation controls brassinosteroid receptor activation by triggering membrane release of its kinase inhibitor. *Genes Dev* 25(3):232–237.
54. Simon MLA, et al. (2013) A multi-colour/multi-affinity marker set to visualize phosphoinositide dynamics in Arabidopsis. *Plant J* 77(2):322–337.
55. Nito K, Wong CCL, Yates JR, 3rd, Chory J (2013) Tyrosine phosphorylation regulates the activity of phytochrome photoreceptors. *Cell Rep* 3(6):1970–1979.